Aswan University Journal of Science and Technology Volume 3, issue 2, December 2023

Analysis of Elastic Scattering $^{32}S + ^{28}Si$ at Energies from 77.0 to 135.0 MeV

A. Hemmdan[1,], Kassem O. Behairy[1], M. A. Hassanain[2], Norhan M. Nazem[1] and M. Anwar[1]*
[1] *Physics Department, Aswan University, Aswan 81528, Egypt*
[2] *Physics Department, New-Valley University, El-Kharga 72516, Egypt*

Abstract: The angular distributions of ^{32}S elastic scattering on ^{28}Si has been analyzed at the energies 77.0, 90.0, 97.09, 120.0 and 135.0MeV in the framework of double folding (DF) model. Two semi-microscopic potentials were generated to analyze the elastic scattering: the real cluster potential model for both nuclei is 8α for the ^{32}S nucleus and ^{28}Si as 7α is constructed, the real of the density independent zero-range M3Y-Raid potential. These two semi-microscopic potentials were compared to those of Woods-Saxon. The imaginary potential part of the three potentials is considered in Woods-Saxon form. Successfully reproduction of the angular distribution cross sections using the three generated potentials is obtained except for the energy 97.09 MeV at backward angles. This disagreement is due to the transfer processes of the α-alpha particle which causes the oscillation curve. The nuclear matter and cluster densities are taken in three Fermi parameters. The energy dependence of the volume integrals and total reaction cross section were also investigated.

Keywords: Optical potential model; folding cluster model; M3Y-Reid interaction; Elastic and Inelastic scattering; Coupled channels.

1. Introduction

The elastic study of peripheral heavy ion (HI) collisions plays a significant role in the overall understanding of heavy ion reactions. One of the goals of studying HI reactions is to determine the form of the most suitable effective nucleon- nucleon potential to explain experimental elastic scattering cross-section data [1]. For many years, using the empirical

Corresponding author E-mail: ahemdan@aswu.edu.eg

Received October 7, 2023 received in revised form November 11, 2023, accepted November 19, 2023.
(ASWJST 2023/ printed ISSN: 2735-3087 and on-line ISSN: 2735-3095) https://journals.aswu.edu.eg/stjournal

parameterization of nuclear potential has been very common in HI studies, but it is desirable to relate the nucleus-nucleus (NN) interactions to the nucleon-nucleon (NN) nuclear potential [2], and many types of potentials have been used to describe the interaction between nuclei. The Optical potential model has been one of them which considered as an effective potential described the reaction between nuclei simply and more accuracy.

The concept of optical model was introduced by Ostrofsky.et al.[3]. In a study of alpha decay from radioactive nuclei, low-energy nuclear compound nuclear reactions were described. This model has been successfully employed to compute the potential between interacting nuclei and describes the most important physical quantities that characterize the properties of nuclear reactions, namely the differential cross-section, polarization, and total nuclear reaction cross-section [4]. The optical potential model mechanism is expressed in reducing the many-body scattering problem consisting of the projectile and composite target to a simpler two-body system and deliberates with the interaction between two beams of the nucleus. Therefore, this model is considered to be the most successful model for understanding nucleus- nucleus interactions through the analysis of elastic and inelastic heavy ion (HI)scattering, and it is an adequate method for the formulation of coupled channels that accompany heavy ion reactions [5].The transparent relationship between the optical potential of the HI and NN interaction has been obtained using the Double Folding (DF) optical potential model, which builds on a realistic effective NN interaction folded with the nuclear matter distributions of the projectile and target nuclei [4]. The folding potentials make it possible to eliminate ambiguities, which appear with the phenomenological potential.

Many attempts in this direction have been made, and recently, the double-folding (DF) model has been extensively used by many groups to describe HI scattering, as it provides a simple possibility of numerical handling in two-nucleus scattering calculations [5]. On the other hand, the double folding cluster (DFC) model has been proven to be quite successful in the analyses of the elastic scattering of various α-clustering nuclei such as ^{12}C, ^{16}O, ^{20}Ne, ^{24}Mg, ^{28}Si, ^{32}S and so on [6–13] based on an α-α interaction folded with the α-particle distributions in the colliding nuclei. This is one of our footings. A recent review of this subject can be found in [1] and references therein. Satchler and Love [5] presented the first successful intensive study to analyze light and heavy composite ion-scattering data using DF optical potentials. In 1987 B.BILWES et al. [14] studied the normalization effect on the differential cross-section behavior using two different potentials M3Y and DDD for the reaction ^{32}S+^{32}S at 77.0, 90.0, 97.09, 120.0, and 160 MeV, and showed that both interactions need to be renormalized by an energy-dependent coefficient to obtain satisfactory

data. In 2002, El-Azab Farid et al. [8] highlighted the importance of the renormalization parameter to obtain a good agreement behavior, so they tasted two potential double folding cluster (DFC) and M3Y for $^{32}S+^{24}Mg$ elastic scattering reactions at five sites of energies (65, 75, 86, 95, and 110.0 MeV). They observed the reverse relation between the renormalization factor and incident energy. The renormalization coefficient is important for obtaining successful data reproduction. El-Azab Farid et al. [6] analyzed the elastic scattering of some heavy ions to construct DFC potentials based on an effective α –n interaction considering the α-cluster density of the projectile nucleus.

To extend the microscopic understanding of previous studies in explaining the scattering of sd-shell nuclei, the elastic $^{32}S+^{28}Si$ scattering was investigated in the present work. The DFC models and DFM with the M3Y-Reid NN interactions in addition to WS potentials were used to analyze this reaction over the energy range of 77-135 MeV. In addition, a bright view of the total reaction cross-section was presented for the considered reaction. This work is organized as follows: A brief description of the derived formalisms and the procedures are given in Sections 2 and 3, respectively. Section 4 is devoted to the results and discussion. Finally, conclusions are presented in Sec. V.

2. Theoretical formalism:

The total nuclear potential that is used to analyze the considered reactions can be written as;

$$U(R) = V_C(R) + V_N(R) \quad (1)$$

where, $V_C(R)$ is the Coloumb potential which taken as a uniform charged sphere of radius $R_C = 1.2\ (A_T^{1/3} + A_P^{1/3})$, $A_T$and A_P are the masses of target and projectile, respectively.

In the present work, the nuclear potential calculations of the$^{32}S+^{28}Si$ elastic scattering were obtained using the optical potential model (OPM) in three forms:

The first form of the potential is taken in the complex WS shape as:

$$V_N(R) = = V_O[1 + \exp(\frac{R-R_V}{a_V})]^{-1} + i\, W_O[1 + \exp(\frac{R-R_W}{a_W})]^{-1} \quad (2)$$

The parameters, $V_0(W_O)$, R_V (R_W) and a_V (a_W) are the depth, radius, and diffuseness of the real (imaginary) potential, respectively. The obtained potential denoted as WS.

The second form of the real part of the OP calculated using the DF model [15] is:

$$V_{DF}(R) = (N_R) \int\int \rho_P(r_1)\rho_T(r_2)v_{NN}(s)dr_1\, dr_2. \quad (3)$$

where,N_R, is the real normalization factor. $\rho_P(r_1)$,$\rho_T(r_2)$ are nuclear matter distribution for the projectile and target respectively while $v_{NN}(s)$ is the nucleon- nucleon interaction potential. The nuclear matter densities assumed to have the same distribution as the charge densities, because

the existence evidence that this hold for s-d nuclei[16]. In the present work, we have used three Fermi parameters form (3pF):

$$\rho(r) = \rho_o(1 + w(\frac{r}{z})^2)(1 + \exp(\frac{r-z}{\beta}))^{-1} \text{ fm}^{-3} \quad (4)$$

The density parameters w, z and β are given in Table (1), which are taken from [17].The effective NN interaction $v_{NN}(s)$ is taken as the density independent M3Y as:

$$v_{nn}(s) = 7999\frac{\exp(4s)}{4s} - 2134\frac{\exp(2.5s)}{2.5s} + J_{oo}(E)\delta \text{ MeV} \quad (5)$$

Where, δ term accounts for knock exchange and $J_{oo}(E)$ is a linearly energy- dependent strength in the form:

$$J_{oo}(E) \approx -276\left[1 - {}^{0.005E}/_{A_P}\right]\text{MeV Fm-3} \quad (6)$$

The third form for the OP real part is constructed based on the α-cluster structure, ^{32}S as (8α) and ^{28}Si as (7α). Consequently, the resulting cluster potential will take the form[6]:

$$V_{DFC}(R) = (N_R)\int\int \rho_{C_P}(r_1)\rho_{C_T}(r_2)v_{\alpha\alpha}(s)dr_1\, dr_2. \quad (7)$$

where, $v_{\alpha\alpha} = -122.6226\exp(-22s^2)$. ρ_{C_P} and ρ_{C_T} are the cluster densities for the projectile and target respectively. Both densities are taken as 3-fermi parameters:

$$\rho_C(r') = \rho_0^c\left(1 + \gamma^c\left(\frac{r'}{Z^c}\right)^2\right)\left[1 + \exp\left(\frac{r'-Z^c}{\alpha^c}\right)\right]^{-1} \quad \text{fm-}^3 \quad (8)$$

The parameters γ^c, Z^c and then $\alpha^c$of the ^{32}S and ^{28}Si α-cluster densities are taken as in ref. [18] and given in Table (1).

Usually, analysis of the HI scattering data using the optical model (OM) is performed using the folded potential as the real part of the optical potential, while the imaginary potential is fitted in a phenomenological form. The imaginary part for the last two potentials is taken as WS form that is represented in Eq. (2).

The volume integral per interacting nucleon pair J is defined as:

$$J_{R,I} = \frac{4\pi}{A_P A_T}\int U_{R,I}(R)R^2 dR \quad (9)$$

The real and the imaginary parts of U(R) is used independently

where $U_{R,I}(R)$ represent the real and imaginary OP parts to obtain the real J_R and the imaginary J_I volume integrals , respectively.

3. Procedures:

The elastic scattering for the reactions of $^{32}S+^{28}Si$ at five sets of energies (77.0, 90.0, 97.09, 120.0, and 135.0 MeV) has been analyzed with three versions of potentials; two semi-microscopic potentials, M3Y and DFC, and the third is phenomenological one (WS). The calculations were performed using the following procedure:

1. The complex phenomenological potential (WS) was calculated using Eqs. (2) and the two Semi-microscopic potentials (M3Y and DFC) using Eq. (3) and (7) for the elastic $^{32}S+^{28}Si$ scattering. These potentials were computed with the help of DFPOT code[19]
2. The elastic scattering differential cross-sections of the considered experimental data were obtained using HERMIZ [20]and FRESCO [21] program codes using the automatic search option. The quality of agreement with the data can be arbitrated by χ^2scale. The calculations were performed for the considered data with experimental errors of 10% as an average value.

$$\chi^2 = \frac{1}{N}\sum_{i=1}^{N}\left[\frac{\sigma_{th}(\theta_i)-\sigma_{exp}(\theta_i)}{\Delta\sigma_{exp}(\theta_i)}\right]^2 \qquad (10)$$

where,$\sigma_{th}(\theta_i)$and $\sigma_{exp}(\theta_i)$ are the theoretical and experimental differential cross sections, respectively at an angle θ_i, N is the number of angles at which measurements are made and $\Delta\sigma_{exp}(\theta_i)$ is the error associated with $\sigma_{exp}(\theta_i)$.

3. The search was carried out on six parameters of WS (three parameters for the real volume part and three for the imaginary part), while the search in the two aforementioned semi-microscopic potentials was attained by four parameters of, DFC and M3Y, (normalization coefficient and the three parameters of the imaginary part of the WS volume).
4. The results of total reaction cross section (σ_R) and the behavior of the volume integrals (real J_R and imaginaryJ_I) are illustrated.

4. Results and Discussion:

The main purpose of the present work expressed in analyzing the differential cross section of $^{32}S + ^{28}Si$ elastic scattering at energies around the Coulomb barrier at five sets of data, E_{lab}=77.0, 90, 97.09, 120, and 135.0 MeV. The elastic cross section is calculated by using the three considered WS, DFC and M3Y potentials for the real part of the optical potential form.

The densities and potentials that used for the analyses are displayed in fig.1, panel (a) shows the behavior of the density distributions of the projectile ^{32}S; for both semi microscopic potentials

(M3Y and DFC) respectively. We used the same nuclear matter density, 3-femi parameter form, which employed to derive M3Y potential to calculate DFC potential. The difference between densities observed at the small inters nuclear distance and they show an identical behavior at the he.

Panel (b): illustrated the real potential part behavior of the three Ops used in calculations for $^{32}S+^{28}Si$ elastic scattering, WS (Solid curve), M3Y (dash curve) and DFC (dash double dot curve) at the incident energies. We observe from this figure that although the main difference between the potentials is showing up at small inter-nuclear distance which corresponds to the high overlap density of the two colliding nuclei, but all real potentials have the same strength and slope at the surface.

The angular distributions of the five mentioned sets of energies as comparison with the calculated theoretical results are shown in Fig. 2. It is obvious that for the first three energies, our calculations reveal better agreement as comparison with those presented in Ref. [22,23]. The WS potential analysis for the two energies 77.0 and 90 MeV is generated in the present work. The obtained successful fitting with data is apparent for all the extracted new parameters in comparison with the previous phenomenological analysis that given in Ref. [22,23]. In other side, also, successful results are reproduced with the semi-microscopic potentials as shown in Fig. 2. Both potentials produce almost identical predictions and comparable values for the parameter moreover, the derived DFC potential predicted the data better than phenomenological analysis in Ref. [22] and more pronounced in comparable with folding analysis in Ref.[23]. As noticed in Fig. 2, despite this successfully reproduced the data, unreasonable agreement is found for 97.09 MeV at the backward angles. The most probably cause of this disagreement is due to the transfer processes of α-alpha particle [23]. Cluster and nucleon exchange effects have indeed been observed to be dominate at large angle elastic scattering in a number of nuclear systems [24,25].

The obtained parameters, the real and imaginary volume integrals per interacting nucleon pair J_R, J_I as well as both of reaction cross sections and reduction coefficient are listed in Table 2 and demonstrated in Fig. 3. The dispersion relation [1] have been applied to the values of the real and imaginary volume integrals in order to check the consistency between the real and imaginary parts and reproduce the observed energy dependence for them. It is noticed from Fig. 3 panel (a) that the real volume integrals of DFC potential have clear energy dependence in compared with M3Y potential, where J_R decreases as energy increases obeying the dispersion relation line. While the imaginary volume integral strength J_I of both potentials increases rapidly to follow the trend of

the dispersion relation curve as shown in panel (b). The extremely small values of the imaginary volume integral as comparison with real part due to the surface scattering which character this type of heavy ions reaction at this range of energy. Moreover, the energy dependence of the total reaction cross section σ_R that calculated from the present analysis compared with the previous results of Ref. [26] are shown in the panel (c). As noticed from this panel, (c), the linear fit with equation $\sigma_R = 2.092 + 0.01E_{lab}$, of the calculated results is reflects the energy dependence of the total reaction cross sectionσ_R. Also, the consistency of the obtained calculations with previously results reflects the success of the present generated potentials.

5. Conclusion

Differential cross sections of elastic scattering for the $^{32}S + ^{28}Si$ system at incident energies around the Coulomb barrier of 77, 90, 97.03, 120, and 135 MeV in the framework of the optical model are analyzed. A successful description of the considered experimental data for elastic scattering was presented using WS as a traditional phenomenological potential, in addition to DFC and M3Y semi-microscopic optical potentials. The DFC potential, which was constructed based on the cluster structure of two colliding nuclei (^{32}S ,^{28}Si) as (8α, 7α) , was considered to generate the real potential. The M3Y potential was compared with the DFC potential. The imaginary part of the two derived potentials was used as the phenomenological WS form. The conclusion from this analysis is that, the optical potentials used in this study are in good agreement with the experimental elastic scattering angular distribution. Successful reproduction of both semi-microscopic potentials for the elastic scattering differential cross-sections is obtained using a normalized real part of their optical potential form.

The present results for the elastic cross section are better than those of the previous WS analysis [22], while they are more pronounced than those of previous CE [26] and M3Y [26] potentials. Moreover, both potentials DFC and M3Y show compatible behavior.

References:

1. M.-E. Brandan and G. R. Satchler, Phys. Rep. **285**, 143 (1997).

2. Zhang Gao-Long, Liu Hao, and Le Xiao-Yun, Chinese Phys. B **18**, 136 (2009).

3. M. Ostrofsky, G. Breit, and D. P. Johnson, Phys. Rev. **49**, 22 (1936).

4. H. Hamagaki, O. Hashimoto, N. Yoshikawa, O. Yamakawa, and N. Takahashi, **55**, 2676 (1985).

5. G. R. Satchler and W. G. Love, Phys. Rep. **55**, 183 (1979).

6. M. E.-A. Farid, Z. M. M. Mahmoud, and G. S. Hassan, Nucl. Phys. A **691**, 671 (2001).

7. M. El-Azab Farid, Z. M. M. Mahmoud, and G. S. Hassan, Phys. Rev. C - Nucl. Phys. **64**, 143101 (2001).

8. M. El-Azab Farid, Phys. Rev. C **65**, 67303 (2002).

9. M. Karakoc and I. Boztosun, Phys. Rev. C **73**, 47601 (2006).

10. Y.-X. Yang and Q.-R. Li, Phys. Rev. C **84**, 14602 (2011).

11. M. A. Hassanain, A. A. Ibraheem, and M. E.-A. Farid, Phys. Rev. C **77**, 34601 (2008).

12. M. A. Hassanain, A. A. Ibraheem, S. M. M. Al Sebiey, S. R. Mokhtar, M. A. Zaki, Z. M. M. Mahmoud, K. O. Behairy, and M. E. A. Farid, Phys. Rev. C - Nucl. Phys. **87**, (2013).

13. D. M. Brink and J. J. Castro, Nucl. Phys. A **216**, 109 (1973).

14. B. Bilwes, R. Bilwes, L. Stuttge, U. L. Pasteur, J. Diaz, J. L. Ferrero, C. Roldan, F. Sanchez, D. F. Corpuscular, F. Ballester, J. Diaz, J. L. Ferrero, C. Roldan, F. Sanchez, U. L. Pasteur, J. Diaz, J. L. Ferrero, C. Roldan, F. Sanchez, and D. F. Corpuscular, Nucl. Phys. A **473**, 353 (1987).

15. A. Hemmdan, M. A. Hassanain, M. Anwar, and K. O. Behairy, Phys. Rev. C **104**, 1 (2021).

16. B. Bilwes, R. Bilwes, J. Diaz, and J. L. Ferrero, Nucl. Physics, Sect. A **449**, 519 (1986).

17. B. Bilwes, R. Bilwes, J. Díaz, J. L. Ferrero, J. C. Pacheco, and J. A. Ruiz, Nucl. Physics, Sect. A **484**, 174 (1988).

18. Z. M. M. Mahmoud, K. O. Behairy, A. A. Ibraheem, S. R. Mokhtar, M. A. Hassanain, and M. El-Azab Farid, J. Phys. Soc. Japan **88**, 1 (2019).

19. J. Cook, Comput. Phys. Commun.;(Netherlands) **25**, (1982).

20. J. Cook, Comput. Phys. Commun. **31**, 363 (1984).

21. I. J. Thompson, Comput. Phys. Reports **7**, 167 (1988).

22. A. Baeza, B. Bilwes, R. Bilwes, J. Diaz, J. L. Ferrero, and J. Raynal, Nucl. Phys. A **437**, 93 (1985).

23. B. Bilwes, R. Bilwes, J. Díaz, J. L. Ferrero, D. Počanić, and L. Stuttgé, Nucl. Phys. A **463**, 731 (1987).

24. L. Jarczyk, J. Okołowicz, A. Strzałkowski, K. Bodek, M. Hugi, L. Lang, R. Müller, and E. Ungricht, Nucl. Phys. A **316**, 139 (1979).

25. W. von Oertzen and H. G. Bohlen, Phys. Rep. **19**, 1 (1975).

26. B. Bilwes, R. Bilwes, J. Diaz, J. L. Ferrero, J. C. Pacheco, and J. A. Ruiz, Nucl. Phys. A **484**, 174

(1988).

Table 1. The 3pF matter (cluster) densities parameters and rms for the ^{32}S, ^{28}Si and ^{16}O:

Nucleus	$\omega(\gamma^C)$	$z(z^C)$[fm]	β (α^C) [fm]	rms [fm]
^{32}S	-0.213(0.234)	3.441(3.137)	0.624(0.274)	3.24(2.87)
^{28}Si	-0.149(0.230)	3.239(3.055)	0.574(0.259)	3.13(2.77)

Table 2 Optical model parameters obtained from the analysis of the 32S + 28Si elastic scattering.

E (MeV)	Pot.	N_R	V (MeV)	r_R (fm)	a_R (fm)	$-J_R$ **(MeV fm^{-3})**	W (MeV)	rI (fm)	aI (fm)	$-J_I$ **(MeV fm^{-3})**	σ_R (mb)	χ^2
	WS		17.3	1.384	0.495	52.86	2.352	1.604	0.11	10.89	417.4	0.69
77.0	M3Y	1.0				419.4	2.82	1.585	0.13	12.61	405.2	0.712
	DFC	1.0				427.2	2.65	1.63	0.11	12.38	439.8	0.712
	WS		36.2	1.3	0.425	94.39	2.265	1.0	1.488	4.026	813.0	4.784
90.0	M3Y	0.77				326.1	2.266	1.59	0.25	12.23	879.8	6.2
	DFC	1.04				444.2	2.42	1.6	0.267	12.28	861.1	5.47
	WS		41.15	1.255	0.497	94.78	2.95	0.93	1.322	4.022	848.1	10.0
97.09	M3Y	0.73				304.8	3.875	1.43	0.435	13.0	873.3	13.0
	DFC	0.8				330.8	4.40	1.321	0.587	11.94	839.1	11.2
	WS		76.64	1.06	0.66	111.9	2.023	1.59	0.415	9.269	1392	2.4
120.0	M3y	0.8				333.2	4.2	1.38	0.446	12.70	1185	3.1
	CDF	0.9				377.2	5.153	1.327	0.532	14.04	1197	2.6
	WS		176.88	1.076	0.684	272.4	5.28	1.39	0.606	38.32	1542	0.33
135.0	M3Y	0.78				323.5	8.96	1.33	0.573	24.64	1486	0.451
	CDF	0.88				363.0	10.63	1.28	0.665	26.39	1522	0.332

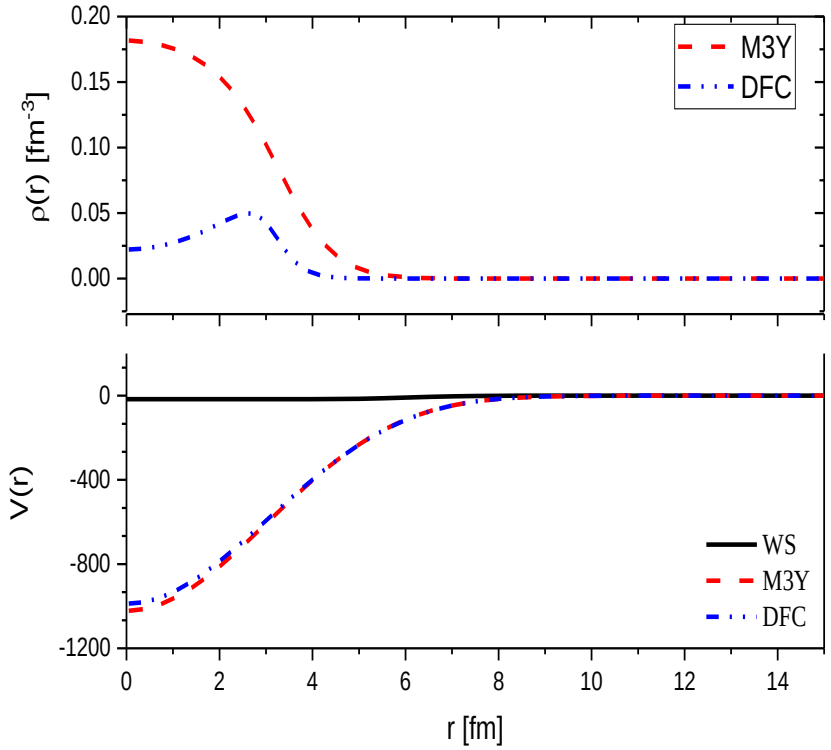

FIG.1 panel (a): nuclear density distributions of the ^{32}S projectile; the dash line for 3pF matter density and the dash double dot refer the 8α cluster density distribution. Panel (b): the real part of the three Ops for ^{32}S+^{28}Si elastic scattering, WS (Solid curve), M3Y (dash curve) and DFC (dash double dot curve)

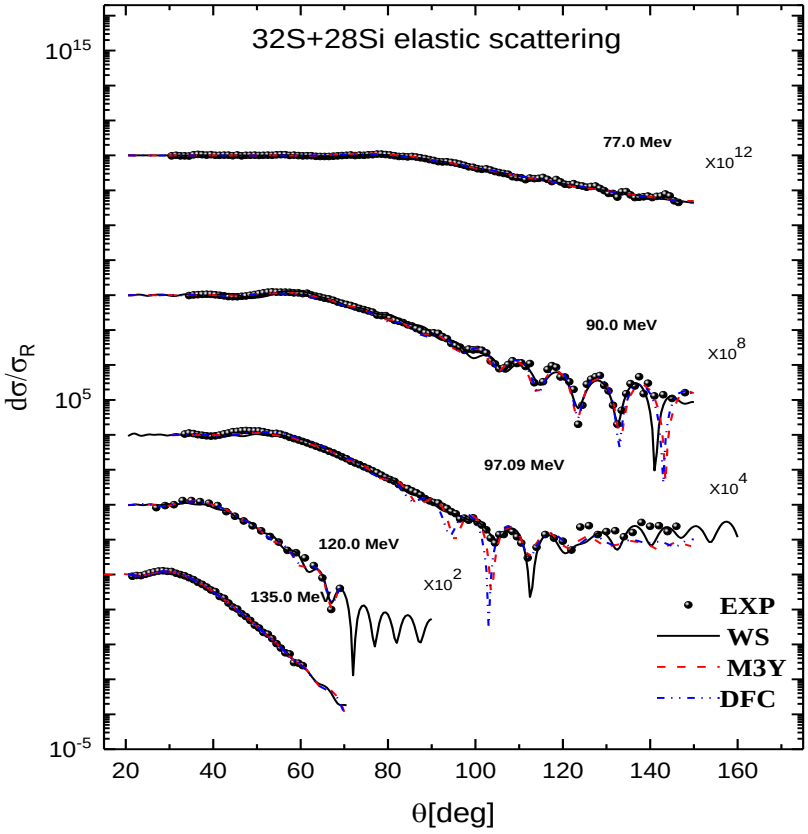

FIG. 2. The experimental elastic angular distribution for $^{32}S+^{28}Si$ scattering at the energies 77.0, 90.0, 97.09, 120.0 and 135.0 MeV in comparison to the theoretical predictions using the optical WS (solid line), M3Y (dash line), and DFC (dash double dot line). The experimental data are taken from ref. [22,23].

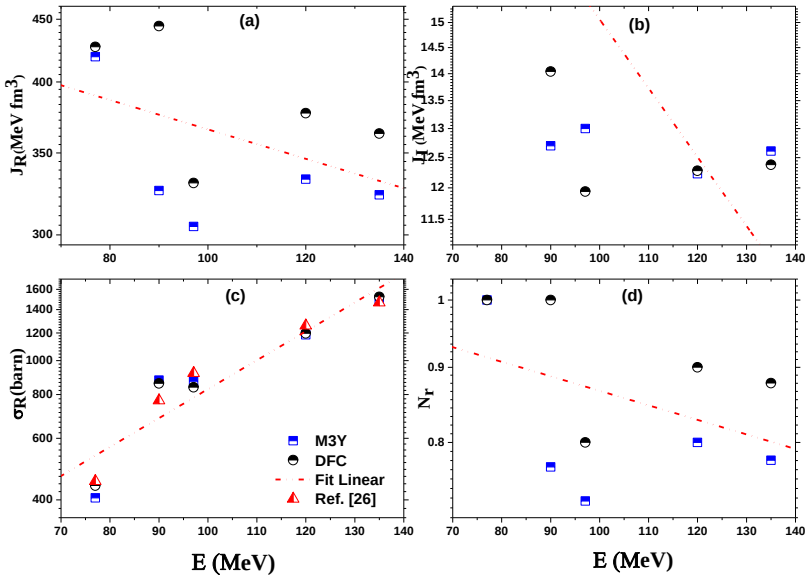

Fig 3. Panel (a) and Panel (b) show the energy dependency of the volume integral of the real J_R and imaginary part J_I in comparison to the dispersion relation between real and imaginary components of the nuclear potentials (sold lines). Panel (c) shows the energy dependence of the total reaction cross section, σ_R in comparison to the results of ref. [26]. Panel (d) shows the energy dependence of the renormalization factor N_r.